

COMPUTER MODELLING OF MATERIALS PROPERTIES

N. Saunders, X. Li, A. P. Miodownik and J-Ph. Schillé

Thermotech Ltd., Surrey Technology Centre
The Surrey Research Park, Guildford GU2 7YG, U.K.

Abstract

Work is being undertaken at Thermotech on the development of a new multi-platform software programme called JMatPro for predicting a wide range of Materials Properties. These properties include thermo-physical and physical properties, mechanical properties, TTT/CCT diagrams etc. and the calculations are being applied to a variety of multi-component alloy types, such as Ni-based superalloys, steels, Ti-alloys, Al-alloys. The new programme is particularly aimed at multi-component alloys used in industrial practice and numerous examples of calculated results for the various properties will be presented with the emphasis being on validation of calculated results against experimental observation.

Introduction

Thermodynamic modelling tools for exploring the equilibrium and phase relationships in complex materials have become increasingly used in actual industrial practice [1]. These tools provide benefit, but their applicability often falls short from directly providing the information that is actually required. For example, thermodynamic modelling helps towards the understanding of changes in phase constitution of a material as a function of composition or temperature. However, there is then a jump in translating this information into the properties being targeted by the end user, e.g. TTT diagrams, mechanical properties, thermo-physical and physical properties.

The left hand side of Fig.1 shows a flow chart of the process that is usually undergone when only a thermodynamic calculation is used in a design process. The jump from thermodynamic calculation to the final understanding of materials properties is a significant one. It can only be achieved through further experimentation if quantitative information is required or through the knowledge and experience of the user if guidance of a more qualitative nature will suffice.

To overcome these limitations a new computer programme has been developed, called JMatPro, an acronym for **J**ava-based **M**aterials **P**roperties software. The approach adopted in the development of the new programme has been to augment the thermodynamic calculation by incorporating various theoretical models and properties databases that will make a quantitative calculation for the requisite materials property within a larger software structure. This then enables a clear path to be created between the thermodynamic calculation and the final product that is required, i.e. the materials property itself. This path is shown by the right hand side of Fig.1.

The new software programme also has as its goal, that it can be used by any engineer or scientist that requires materials properties as part of their everyday work. To this end, not only must sound predictions of such properties be made by the software programme, the user should not require advanced computer skills to operate it. Following modern software practice, there should also be an extensive on-line help facility so that the user can familiarise themselves with the programme without the need to read weighty user manuals. Further, the new programme should be platform independent, able to run on Windows'98/NT/2000, Linux, Unix based workstations, etc.. To this end,

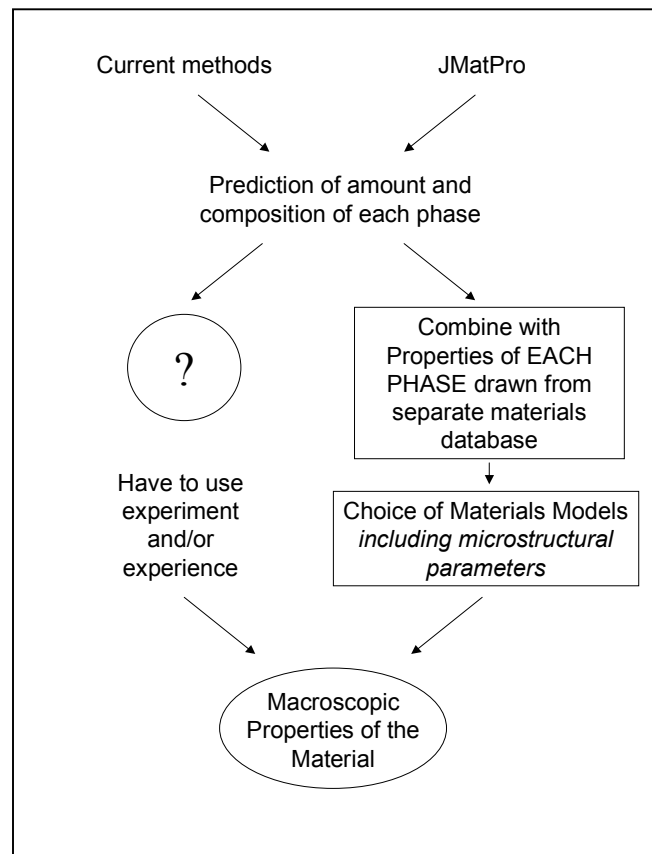


Figure 1: Diagram showing flow chart for how materials properties are obtained using (i) the current application of thermodynamic calculations and (ii) the route used by JMatPro

the software structure combines a Java based GUI with scientific software written using C/C++ for ease of portability.

The purpose of the present paper is to describe the capability of the programme, giving extensive examples of its application to multi-component commercial alloys, with particular emphasis on the validation of the calculated property against experiment. The properties that will be dealt with will include,

1. Thermodynamic calculations
2. Thermo-physical and physical properties
3. Phase transformations
4. Mechanical Properties.

Results and Discussion

Thermodynamic calculations

The current software utilises core minimisation routines developed for the PMLFKT software programme by Lukas et al. [2] and recently extended by Kattner et al. [3] to multi-component alloys. These sub-routines have been converted from Fortran to C and, in addition, a comprehensive set of new sub-routines written in C/C++. These new sub-routines provide (i) facilities for setting automatic start points, (ii) original algorithms to ensure that highly reliable results for multi-component, multi-phase equilibria can be routinely calculated, (iii) algorithms for stability checking that also continually monitor the composition of the various phases that may have miscibility gaps or the potential for ordering, (iv) highly robust routines for finding phase boundaries etc.. A sample calculation for a duplex stainless steel is shown in Figure 2, below.

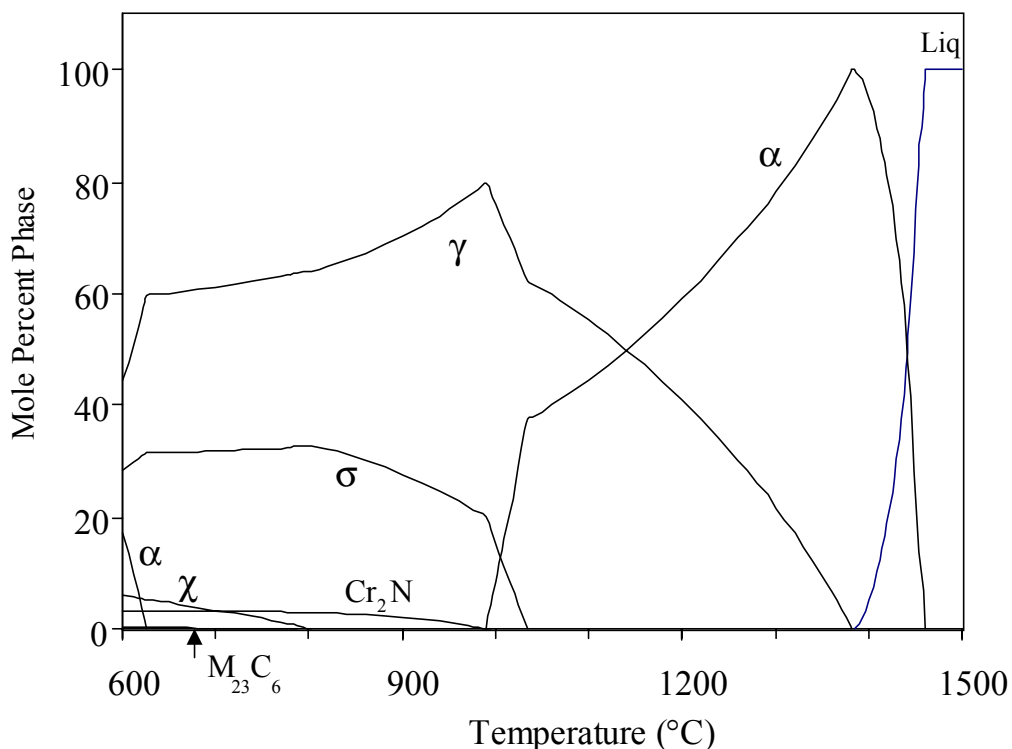


Figure 2: Calculated amount of phase vs. temperature plot for a SAF 2507 Duplex stainless steel

2.2 Thermo-physical and Physical Properties

Thermo-physical and physical properties are an important part of materials science, particularly at the present time when such data is critical input for new software programmes dealing with process modelling. Currently, the following properties are being considered in the programme, Young's (E), Shear (G) and Bulk (K) moduli, Poisson's ratio, Thermal conductivity, Thermal expansion coefficient and Density. Assessment work has already started for building up the requisite materials databases and some of this work has been reported already [4, 5].

Temperature(°C)	25.0	100.0	200.0	300.0	400.0	500.0
Young's Modulus (E) (GPa)	108.0	104.26	99.27	94.28	89.29	84.3
Bulk Modulus (K) (GPa)	118.04	113.95	108.49	103.04	97.59	92.14
Shear Modulus (G) (GPa)	40.07	38.69	36.83	34.98	33.13	31.28
Poisson's Ratio	0.35	0.35	0.35	0.35	0.35	0.35
Thermal Conductivity (W/m/K)	5.35	6.81	8.4	9.78	11.04	12.23
Thermal Expansion (1/K)	9.97E-6	1.03E-5	1.07E-5	1.11E-5	1.16E-5	1.2E-5
Density (g/cm ³)	4.54	4.53	4.51	4.49	4.47	4.45

Figure 3: Results from JMatPro showing various physical properties, including their variation with temperature, for a mill annealed SP700 α/β Ti-alloy.

Figure 3 shows a results from JMatPro providing various physical properties (including their variation with temperature) for a SP700 α/β Ti-alloy in the mill-annealed (720°C) condition. To confirm the validity of the output, Figs.4&5 show respectively, plots comparing experimentally measured and calculated Young's Modulus and thermal conductivity for a large number of commercial Ti-alloys. It can be seen that there is excellent agreement between calculation and experiment and it is noted the temperature dependence of these properties has been included. Similar properties are also calculated for steels and Ni-based superalloys with excellent success.

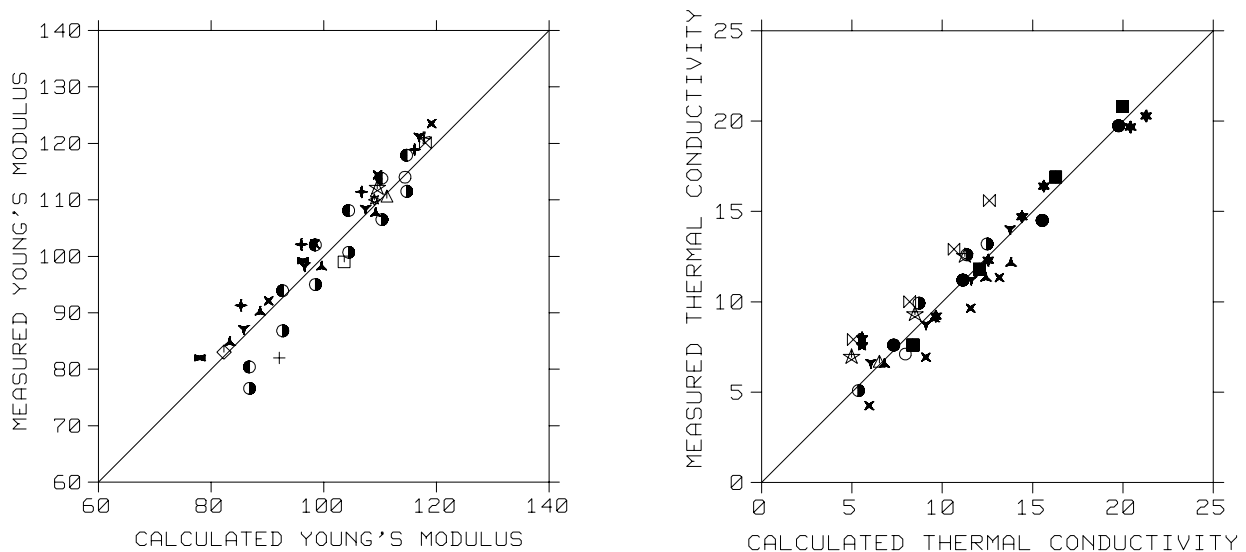


Figure 4: Comparison between calculated and experimentally measured (a) Young's modulus and (b) thermal conductivity in commercial Ti-alloys.

Phase Transformations

The evolution of volume fraction during solid-state transformation can be described using the well known Johnson-Mehl-Avrami equation, which, for spherical particles and isothermal conditions, can be expressed as [6]

$$x = \frac{V}{V_{\text{eq}}(T)} = 1 - \exp\left(-\frac{\pi}{3} N_r G_r^3 t^4\right) \quad (1)$$

where T is the temperature, V is the volume fraction transformed at time t , V_{eq} is the equilibrium amount of precipitate, N_r is the nucleation rate and G_r is the growth rate. A more general form is usually used in practice, taking the form

$$x = 1 - \exp(-k t^n) \quad (2)$$

where k is a constant, subsuming effects associated with nucleation and growth, and is usually empirically evaluated for each temperature. n is the time exponent, often called the Avrami exponent. In order for eq.2 to be applied successfully, it has long been known that n can vary anywhere between 1-4. The various values of n are usually linked to factors such as shape of the precipitate, whether the nucleation or growth rate is constant or varying with time or nucleant site saturation has been achieved.

The main aim of the present work has been to include a more explicit representation of nucleation and growth rates as shown in eq.1 while maintaining the flexibility of approach more inherent in the generalised form shown in eq.2. This has been achieved by including a more explicit incorporation of the effect of shape in the basic equations after Martin *et al* [7]. Work has been undertaken to build up the requisite diffusion databases, assess the various nucleation and shape characteristics for the various types of precipitate and validate the approach by comparison with experiment. A significant factor in the success of the approach has been the capacity to extract explicit values for transformation temperatures, equilibrium amounts and compositions for the precipitating phase, and allied thermodynamic factors such as driving forces from thermodynamic calculation. A more detailed explanation of the approach will be presented later [8].

An advantage of the current modelling method is that few input parameters need to be empirically evaluated. Where empirical values are used, for example in consideration of shape and nucleant density, specific values have been defined for the various precipitates (i.e. σ , χ , μ , α -Ti) in each material type. Once these values are defined, they have then been self-consistently applied and the model can therefore be used in a predictive fashion.

Formation of topologically close packed (TCP) phases: The precipitation of topologically close packed (TCP) phases such as σ , μ , χ and Laves is an important factor in both service and processing and it is therefore of great interest to be able to predict the kinetics of transformation of these phases. Their formation is especially important in Ni-based superalloys and stainless steels, where their formation is usually associated with factors such as embrittlement, loss of creep strength, degradation of pitting resistance etc.. To this end, models for these types of alloys have been developed.

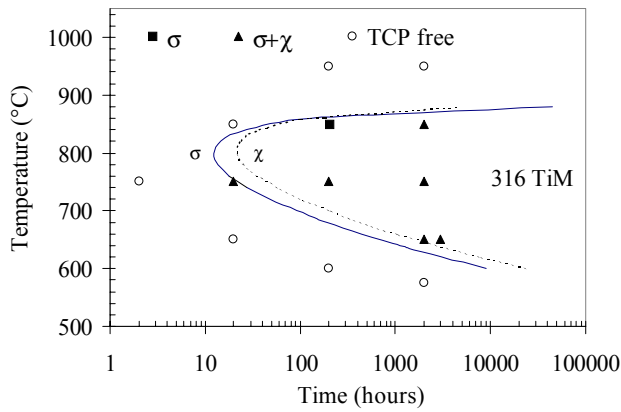


Figure 5: Comparison between calculated and experimentally observed [9] TTT diagram for a 316 austenitic stainless steel

Figure 5 shows the comparison between experimentally observed [9] and calculated behaviour transformation behaviour in a 316 austenitic stainless steel. The curves are calculated for 0.5% transformation of σ and χ . Both of these phases form in the alloy and their calculated transformation kinetics are very similar as might be expected. The agreement with overall behaviour is rather good and rather typical of the accuracy that can be obtained.

Other TTT studies more clearly show the competition that can exist between various phases. For example, Figure 6 shows a comparison between observed [10] and calculated transformation behaviour in a Rene N18, Ni-based superalloy. In this alloy, μ is the stable TCP phase. However, σ is the first phase to form, and then transforms to μ . In the calculations, both the rate of transformation is reasonably well matched as well as σ having the fastest transformation kinetics. A similar feature is observed in duplex stainless steels (DSS), where σ is the most stable TCP phase, but a Mo-rich χ phase can form preferentially in certain temperature ranges. Figure 7 shows a similar comparison between calculated and observed transformation behaviour [11]. For both cases, the faster transformation rate of the less thermodynamically stable phase is considered due to the existence of more abundant heterogeneous nucleation sites.

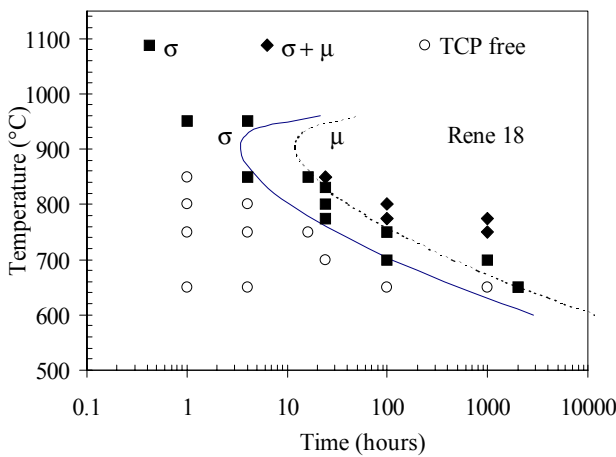


Figure 7: Comparison between calculated and experimentally observed [10] TTT diagram for a Rene N18 Ni-based superalloy

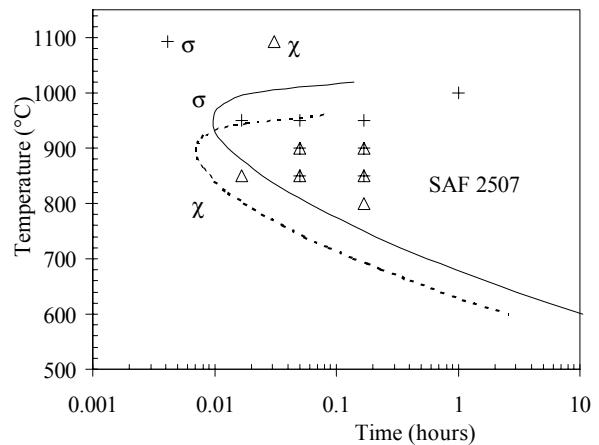


Figure 6: Comparison between calculated and experimentally observed [11] TTT diagram for a SAF 2507 duplex stainless steel

Formation of γ' and γ'' phases: The present approach has been extended to the transformation kinetics in γ' and γ'' hardened Ni-base superalloys. In this case, spheroidal growth is assumed and a nucleant density of 10^{22} - 10^{23} m^{-3} , similar to that which can be observed in Ni-Al binary alloys [12], is taken. In this case, the start of transformation is associated with particles of approximately 5nm in size, sufficient to provide a hardening response. An example of this type of calculation is shown for a 718 alloy (Figs.8a&b) and comparison made with the reported TTT diagram [13]. Note that the precipitation of δ and σ is also included and matched rather well.

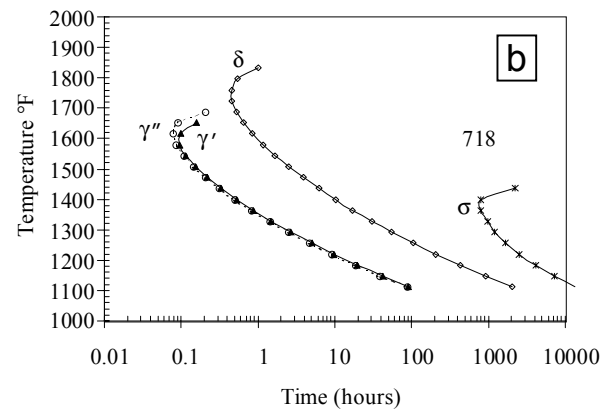
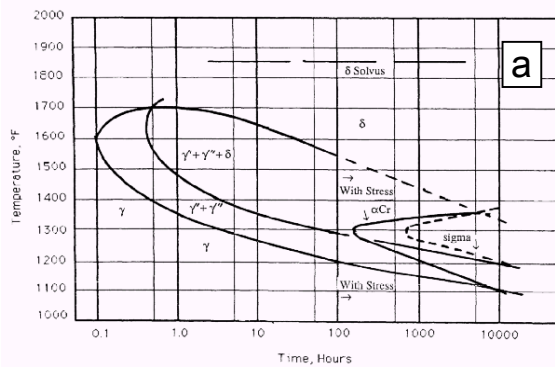


Figure 8: Experimentally observed [13] and calculated TTT diagram for Ni-based superalloy 718.

In the case of such alloys, it may be that nucleant densities are higher and that the onset of readily observable transformation (either through microscopy or a hardening response) is actually associated with coarsening of even finer initial γ'/γ'' particles. This potential case is currently under examination and work presented later in this paper on modelling of precipitate hardening and coarsening will be extended to produce both hardening curves and the associated size of γ' as a function of time. This should enable a better understanding of the exact mechanism that is taking place. However, whichever is the case, the current assumptions provide TTT diagrams in good agreement with observation for alloys such as 718, 625 and 706, and can be immediately be used in design of heat treatment schedules.

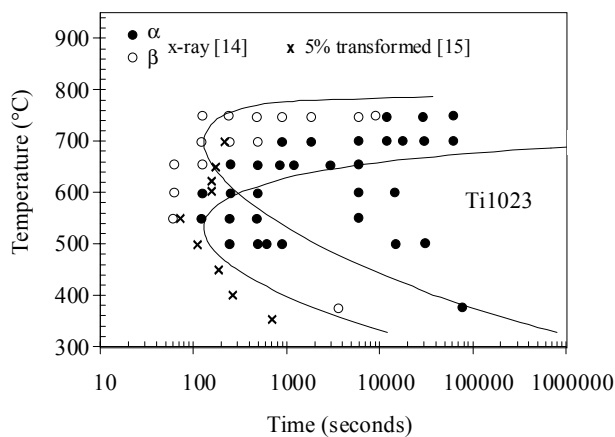


Figure 9: Experimentally observed [14, 15] and calculated TTT diagram for Ti-alloy Ti1023

TTT diagrams for Ti-alloys: Another important area for testing TTT diagrams is in Ti-alloys. In this case, the low temperature allotropic form α -Ti precipitates out from the high temperature β -Ti. Often, nucleation can be observed both at the β grain boundary sites and in the bulk of the prior β grains. To this end, both grain boundary and intra-granular nucleation were simulated by changing the wetting angle function for heterogeneous nucleation and by varying the number of nucleation sites available for growth. It is then possible to calculate two distinct TTT curves. Fig.9 shows such a calculated diagram for a Ti-1023 alloy with experimentally observed points [14, 15] superimposed (Fig.9)

Phase Transformations coupled with Mechanical Properties

TTT/CCT diagrams and Jominy Hardenability in HSLA steels: For the case of HSLA steels, we have adopted a slightly modified approach following Kirkaldy and co-workers [16, 17]. This has proved a reliable method for calculating TTT and CCT diagrams for such alloys, with the significant advantage that hardenability can also be treated. Figure 10 shows a calculated CCT diagrams for US4140 while Figure 11 shows the associated

calculated Jominy hardenability curve with experimental values [18] points shown for comparison. A wide range of alloys has been tested with excellent success. In the future, we will be looking into methods that more explicitly calculate volume fractions of the various phases in HSLA steels, with the intention of expanding the number of properties that can be calculated.

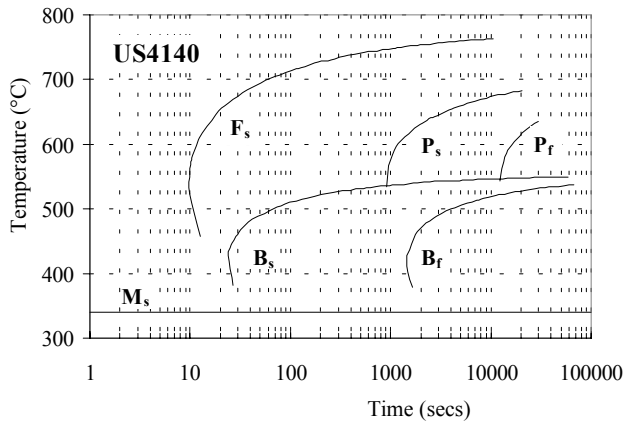


Figure 10: Calculated CCT diagram for a US4140 steel

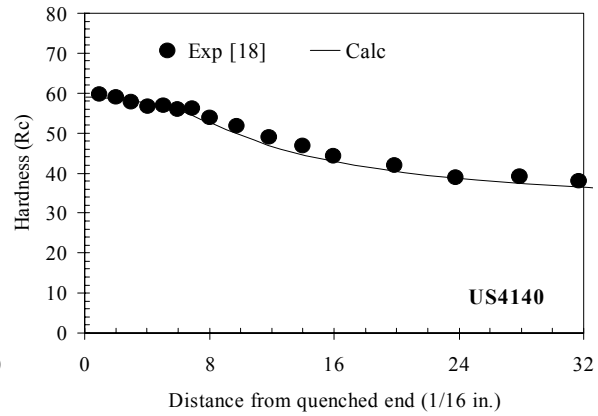


Figure 11: Comparison between calculated and observed Jominy hardness for a US4140 steel

Ductile/brittle Transformation in Duplex Stainless Steels: Substantial experimental work has been done to show the effects of the σ -phase on the mechanical properties of duplex stainless steels [19, 20, 21]. In particular, Charpy testing has been performed on isothermally transformed material to observe the sharp decrease of toughness that occurs at quite early stages of σ phase transformation. To this end, TTT diagrams at various amounts of σ transformation have been calculated for duplex stainless steels with the aim of comparing with known Charpy results. Figure 12 shows the correlation between the calculated TTT diagrams at 5 and 10% amount of σ -phase and Charpy test data for SAF 2205 [20].

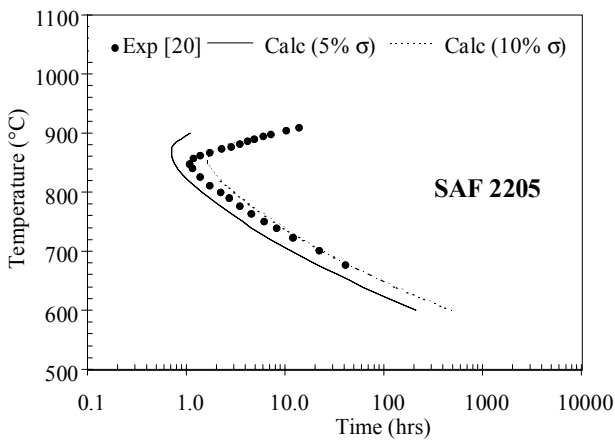


Figure 12: Calculated TTT diagram at 5% and 10% σ -phase formation in SAF 2205 with experimentally observed ductile/brittle transition [20].

The experimental curve represents an impact energy of 27 Joules, which is the critical limit for toughness usually accepted by DSS users. The transition occurs between 5 and 10% σ transformed, which is consistent with values postulated from experimental results [22].

Mechanical Properties

Solid Solution Strengthened Alloys: The yield or proof stress of single-phase materials can be calculated using the standard Hall-Petch equation [23]:

$$\sigma_y = \sigma_o + kd^{\frac{1}{2}} \quad (3)$$

Where σ_y is the yield or proof stress, σ_0 is the intrinsic flow stress, k is the Hall-Petch coefficient and d is the grain size. Two types of databases for solid solution hardening have been created; one for flow stress and the other for Hall-Petch coefficients. These databases are similar in format to thermodynamic ones in that they comprise input coefficients for the pure metals and solid solution strengthening coefficients as a function of pair-wise mixing of the various elements. Once the proof stress of solid solution alloys has been calculated, the ultimate tensile stress (UTS) and hardness can be derived from the inter-relationship between the proof stress, hardness and UTS as described previously [5]. Figure 13 shows the agreement between calculated and experimentally observed proof stress of a wide range of solution strengthened alloys while Fig.14 shows a comparison between UTS calculated from the proof stress and experiment.

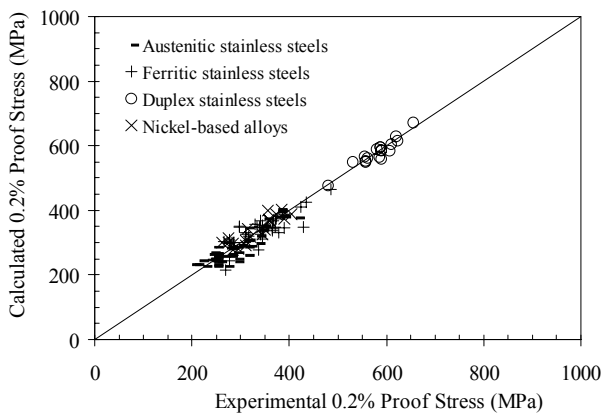


Figure 13: Comparison between calculated and experimentally measured 0.2% proof stress in Fe- and Ni-based solid solution alloys

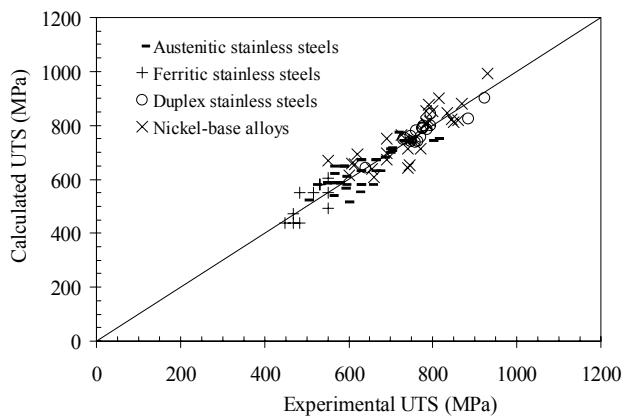


Figure 14: Comparison between UTS derived from calculated 0.2% Proof Stress strengths with experimentally measured values for Fe- and Ni-based solid solution alloys

γ' Hardened Ni-based Superalloys: In Ni-based superalloys strengthened by ordered γ' precipitates, dislocations typically travel in pairs because the passage of a pair of matrix dislocations through a γ' particle restores perfect order on the $\{111\}$ slip plane. When the particle is small, the yield (or proof) stress is determined by the stress that is necessary to move weakly coupled dislocation pairs. In this case, the first dislocation bows out and the second dislocation remains straight. Following Brown and Ham [24] the yield stress can be derived as

$$YS_1 = YS_0 + M \frac{\gamma}{2b} \left[A \left(\frac{\gamma f d}{\tau} \right)^{1/2} - f \right] \quad \dots(4)$$

Where YS_0 is the yield (proof) stress due to solution hardening, M is the Taylor factor [25] that relates the proof stress in polycrystalline material and critical shear stress (CRSS) in single crystal specimens (≈ 3 for FCC materials [25]), γ is the APB energy in the $\{111\}$ plane, b is the burgers vector of dislocation, d is the particle diameter, f is the volume fraction of γ' precipitates, τ is the line tension of the dislocation and A is a numerical factor depending on the morphology of the particles, which for spherical particles equals to 0.72.

When the particles become large, the coupling of the dislocations can become particularly strong because both dislocations may reside in the same particle. Hüther & Reppich [26] have analysed this situation for spherical ordered precipitates and have

derived a formula in which the yield stress (CRSS in original paper) decreases with increasing particle size according to:

$$YS_2 = YS_0 + 1.72M \frac{\tau_f^{1/2}}{2bd} \left(1.28 \frac{\gamma d}{\omega \tau} - 1 \right)^{1/2} \quad \dots(5)$$

The parameter ω accounts for the repulsion of the dislocations within the precipitates, and is essentially an empirically adjustable parameter. For any given particle size, d , the yield stress is governed by the lower of the two values YS_1 and YS_2 because dislocations will tend to move by whichever of the two mechanisms provides the least resistance to glide.

Most of the input into eqs.4&5 can be calculated through an equilibrium thermodynamic calculation and by using the assessed databases for modulus and solid solution strengthening. However, the most critical factor was found to be the APB energy and this was obtained from a thermodynamic calculation route as described previously [27]. Figure 15 shows the typical behaviour associated with hardening by γ' particles as a function of particle diameter; experimental data here are from Mitchell [28]. There is, initially, a steep rise in strength where the deformation mechanism is dominated by small particle effects. A peak is reached, after which the effect of dislocation coupling becomes more important and the strength then decreases with increasing size of γ' particles. Calculations have also been made for a number of commercial superalloys where specific information on γ' size is available (Fig.16). Where size distributions are bi-modal or higher, the amount of γ' at the final heat treatment temperature has been used for the calculation and the total strength obtained by a simple summation of the strengthening effect of the various size distributions [29, 30].

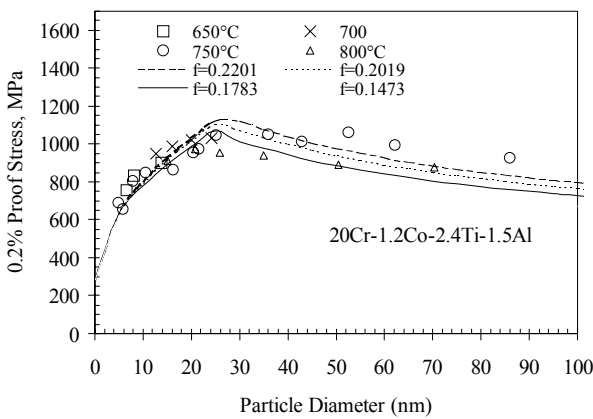


Figure 15: Comparison between calculated and experimental 0.2% Proof Stress as a function of γ' size and volume. γ' amounts are those calculated at the respective ageing temperature.

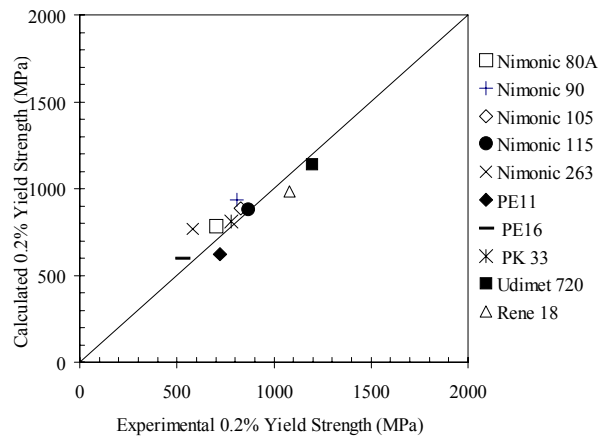


Figure 16: Comparison between calculated and experimental 0.2% Proof Stress of various commercial Ni-based superalloys.

Coarsening of γ' Particles in Ni-based Superalloys

The growth of γ' particles by Ostwald ripening is important for a number of reasons, not least because the final strength of an alloy is dependent on the γ' size. The coarsening of γ' has therefore been simulated to establish a link with the TTT calculations discussed earlier. Ostwald ripening occurs because small particles, which have a high surface energy to volume ratio, are consumed in favour of growth of larger particles in order that

the alloy can reduce its total internal energy. Coarsening is often simulated using an equation of the form:

$$r^3(t) - r_0^3 = kt \quad (6)$$

k can be derived from theoretical considerations such that [7]

$$k = \frac{8D\sigma C_e V_m}{9RT} \quad (7)$$

where r_0 is the mean radius at time $t=0$, D is the diffusion coefficient, σ is the matrix/particle interfacial energy, C_e is the equilibrium solubility of solute in the particles, V_m is the molar volume of the precipitate, R is the gas constant and T is the absolute temperature. This would be equivalent to the model after Lifshitz, Slyozov [31] and Wagner [32] and eqs.6&7 combine to give the well-known LSW equation. A more general form of the LSW equation can be derived as [7]

$$\bar{r}_{(t)}^3 - \bar{r}_0^3 = \frac{8D\sigma N_\alpha (1 - N_\alpha) V_m}{9\varepsilon_\alpha (N_\beta - N_\alpha)^2 RT} t \quad (8)$$

where N_α and N_β are the mole fractions of solute in the matrix and particle respectively and ε_α is the Darken factor. Taking the molar volume of γ' as for Ni_3Al , an approximation that should not significantly affect the accuracy of the final result, all other input are defined or can be obtained either from thermodynamic calculation or the requisite diffusional database. For the case of σ , we have assumed that the matrix/nucleus interfacial energy is related to the enthalpy of solution of γ' in γ [33, 34, 35]. Such a derivation inherently assumes that σ is dominated by chemical, rather than physical effects, such as coherency strains. While it is recognised that such strain energy terms must exist if the γ/γ' interface is coherent or semi-coherent in nature, values for σ of $\sim 20 \text{ mJ m}^{-2}$ are calculated by the current method for various binary Ni-Al alloys which compares favourably with previous experimental studies that suggest values of $14\text{-}30 \text{ mJ m}^{-2}$ [36, 37, 38]. Furthermore, calculated growth rates match experiment so well that we are led to conclude that the calculation method does produce reliable values for σ . Figure 17 shows the comparison between experimentally observed [39, 40, 41, 42, 43] and calculated growth rates of γ' in numerous commercial alloys over wide ranges of temperature. The agreement is quite startling.

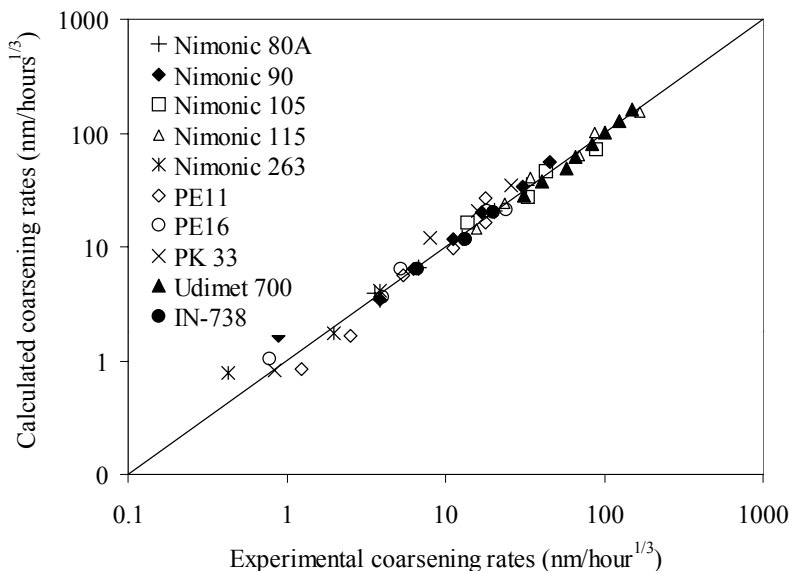


Figure 17: Comparison between calculated and experimentally measured coarsening rates for γ' in Ni-based superalloys

Summary and Conclusions

Results from a new computer programme for calculating general Materials Properties have been presented. The properties that have been tackled are wide-ranging and results have been extensively compared to experiment. They include:

1. The calculation of stable and metastable phase equilibria.
2. Various TTT diagrams for Ti-, Ni- and Fe-based alloys.
3. Hardenability of HSLA steels.
4. The ductile/brittle transition in duplex stainless steels.
5. Proof/tensile strengths and hardness of solution and precipitate strengthened alloys.
6. Coarsening of γ in Ni-based superalloys.

The importance of prior knowledge of phase equilibria and thermodynamics in determining critical input parameters is undoubtedly one of the keys to the success of the present approach and it represents a powerful, new extension to the CALPHAD approach.

References

1. N. Saunders and A.P. Miodownik, *CALPHAD – Calculation of Phase Diagrams, Pergamon Materials Series vol.1*, ed. R.W. Cahn (Oxford: Elsevier Science, 1998).
2. H.L. Lukas, J. Weiss and E.-Th. Henig, *CALPHAD*, 6, (1982), 229.
3. U.R. Kattner, W.J. Boettinger and S. R. Coriell, *Z.Metallkde.*, 87, (1996) , 522.
4. A.P. Miodownik and N. Saunders “*Variation of Elastic Moduli with Composition in Titanium Alloys*”, presented at CALPHAD XXIX, Boston Mass., June 2000-09-13.
5. X. Li, A.P. Miodownik and N. Saunders “*Simultaneous Calculation of Mechanical Properties and Phase Equilibria*”, to be published in *J. Phase Equilibria*.
6. D.A. Porter and K.E. Easterling, *Phase Transformations in Metals and Alloys* (London: Chapman & Hall, 1992).
7. J.W. Martin, R.D. Doherty and B. Cantor B, *Stability of Microstructure in Metallic Systems*, (Cambridge: Cambridge University Press, 1997).
8. X. Li, N. Saunders and A.P. Miodownik, in preparation
9. A.S. Grot and J.E. Spruiell, *Met. Trans. A*, 6A ,(1975), 2023.
10. S.T. Wlodek, M. Kelly and D. Alden, *Superalloys 1992*, Ed. S.D. Antolovich et al. (Warrendale, OH: TMS, 1992), 467.
11. J.O. Nilsson and A. Wilson, *Materials Science and Technology*, 9, (1993), 545.
12. H.I. Aaronson and F.K. LeGoues, *Met. Trans. A*, 23A, (1992), 1915.
13. A. Oradei-Basile, *Superalloys 718, 625 and Various Derivatives (1991)*, Ed. E.A. Loria, (Warrendale, PA: TMS, 1991), 325.
14. S. Bein and J. Bechet, *Titanium '95 Science and Technology (1995)*, eds. P. Bleckinsop et al. (London: The Institute Materials, 1996), 2353.
15. J.R. Toran and R.R. Biederman, *Titanium Science and Technology*, Eds. H. Kimura and O. Izumi, (Warrendale, PA: Met.Soc.AIME, 1980), 1491.
16. J.S. Kirkaldy, B.A. Thomson, and E.A. Baganis, *Hardenability Concepts with Applications to Steel*, eds. J.S. Kirkaldy and D.V. Doane, (Warrendale, PA: AIME, 1978), 82.
17. J.S. Kirkaldy and D.Venugopalan, *Phase Transformations in Ferrous Alloys*, eds. A.R. Marder and J.I. Goldstein, AIME, (Warrendale, PA: AIME, 1984), 125.
18. *Atlas of isothermal transformation and cooling transformation diagrams*, (Metals Park, OH: ASM, 1977), 391.

19. J. Charles, *Duplex stainless steels 94*, ed. T.G. Gooch (Glasgow: The Welding Institute, 1994) paper K1.
20. T. Thorvaldsson, H. Eriksson, J. Kuika and A. Salwen, *Proc. Conf. Stainless Steel 84*, (London: The Institute of Metals, 1985), 101.
21. C.V. Roscoe, K.J. Gradwell and G.W. Lorimer, *Proc. Conf. Stainless Steel 87*, (London: The Institute of Metals, 1988), 563.
22. J.O. Nilsson and A. Wilson, *Materials Science and Technology*, 9, (1993), 545.
23. E.O. Hall, *Yield Point phenomena in Metals and Alloys*, (London: Macmillan, 1970), 38.
24. L.M. Brown and R.K. Ham, *Strengthening Mechanisms in Crystals*, (London: Applied Science, 1971).
25. J.W. Martin, *Precipitation hardening: 2nd Ed.*, (London: Butterworth-Heinemann, 1988), 79.
26. W. Hüther and B. Reppich, *Z. Metallkde.*, 69, (1978), 628.
27. A.P. Miodownik and N. Saunders, *Applications of Thermodynamics in the Synthesis and Processing of Materials*, eds. P. Nash and B. Sundman, (Warrendale, PA: TMS, 1995), 91.
28. V.W.I. Mitchell, *Z. Metallkde.*, 7, (1966), 586-589.
29. B. Reppich, W. Kühlein, G. Meyer, D. Puppel, M. Schulz and G. Schumann, *Mater. Sci. Eng.*, 83, (1986), 45.
30. D.J. Chellman, A.J. Luévano and A.J. Ardell, *Strength of Metals and Alloys*, (London: Freund Publishing House, 1991), 537.
31. I.M. Lifshitz and V.V. Slyozov, *J Phys. Chem. Solids*, 19, (1961), 35.
32. C. Wagner, *Z. Elektrochem*, 65 (1961), 581.
33. N. Saunders and A.P. Miodownik, *Mater. Sci. Tech.*, 4, (1988), 768.
34. D. Turnbull, *Impurities and Imperfections*, American Society for Metals, Cleveland, Ohio, 1955), 121.
35. T. Nishizawa, I. Ohnuma and K. Ishida, *J. Phase Equilibria*, 22, 2001, 269
36. A.J. Ardell, *Acta Met.*, 16, (1968), 511.
37. T. Hirata and D.H. Kirkwood, *Acta Metall.*, 25, (1977), 1425.
38. S.Q. Xiao and P. Haasen, *Acta Metall.*, 39, (1991), 651.
39. W. Betteridge and J. Heslop, *The NIMONIC Alloys and Other Ni-Based High Temperature Alloys: 2nd ed.*, (London: Edward Arnold Ltd, 1974).
40. E.H. van der Molen, J.M. Oblak and O.H. Kriege, *Met. Trans.*, 2, (1971), 1627.
41. K. Bhanu Sankara Rao, V. Seetharaman, S.L. Mannan and P. Rodriguez, *Mater. Sci. Eng.*, 58, (1998), 93.
42. B. Reppich, W. Kühlein, G. Meyer, D. Puppel, M. Schulz and G. Schumann: *Mater. Sci. Eng.*, 83, (1986), 45.
43. R.A. Stevens and P.E. J. Flewitt, *Mater. Sci. Eng.*, 37, (1979), 237.